Effect of Surface Potential Barrier on the Electron Energy Distribution of NEA Photocathodes*

Zou Jijun[1,2], Yang Zhi[2], Qiao Jianliang[2], Chang Benkang[2,†], and Zeng Yiping[3]

(1 *Department of Electronic Engineering, East China Institute of Technology, Fuzhou 344000, China*)
(2 *Institute of Electronic Engineering and Opto-Electronic Technology, Nanjing University of Science and Technology, Nanjing 210094, China*)
(3 *Institute of Semiconductors, Chinese Academy of Sciences, Beijing 100083, China*)

Abstract: By calculating the energy distribution of electrons reaching the photocathode surface and solving the Schrödinger equation that describes the behavior of an electron tunneling through the surface potential barrier, we obtain an equation to calculate the emitted electron energy distribution of transmission-mode NEA GaAs photocathodes. According to the equation, we study the effect of cathode surface potential barrier on the electron energy distribution and find a significant effect of the barrier-Ⅰ thickness or end height, especially the thickness, on the quantum efficiency of the cathode. Barrier Ⅱ has an effect on the electron energy spread, and an increase in the vacuum level will lead to a narrower electron energy spread while sacrificing a certain amount of cathode quantum efficiency. The equation is also used to fit the measured electron energy distribution curve of the transmission-mode cathode and the parameters of the surface barrier are obtained from the fitting. The theoretical curve is in good agreement with the experimental curve.

Key words: NEA photocathode; surface potential barrier; transmission coefficient; electron energy distribution; quantum efficiency
PACC: 7960; 7335C; 7280E
CLC number: TN223 **Document code**: A **Article ID**: 0253-4177(2008)08-1479-05

1 Introduction

A negative-electron-affinity (NEA) photocathode is a cathode in which the vacuum level at the surface lies below the conduction band minimum in the bulk. Therefore, the photoelectrons can diffuse to the cathode surface and tunnel through the surface potential barrier with high probability[1,2]. The NEA state can be achieved by co-adsorption of cesium and oxygen on an Ⅲ-Ⅴ semiconductor, such as GaAs, InP, and GaN. The NEA photocathodes have already found widespread applications in photomultiplier tubes and high-performance image intensifiers in the past several decades because of their high quantum efficiency and good long-wavelength response[1~4]. NEA cathodes are potential sources for next-generation electron accelerators and electron beam lithography due to their high spin polarization and low energy spread and emittance[5~8]. A polarization higher than 80% and a energy spread as low as 40meV have been achieved for NEA GaAs photocathodes[6~8].

Compared with other cathodes, NEA cathodes are a potential electron source with high performance. However, their emitted electron beam properties are still affected by some factors. Revealing the effect of these factors on the electron beam will be significant for the improvement of electron beam performance and the applications of the NEA cathode electron source. Electron energy distribution is an important aspect in the characterization of electron beam performance, which is the main work in this paper. Although there have been many investigations into the electron energy distribution of NEA cathodes[8~11], there are few works concerning the effect of the cathode surface barrier on the distribution. By calculating the energy distribution of electrons reaching the cathode surface and solving the Schrödinger equation for an electron tunneling through the surface potential barrier, we obtain an equation to calculate the emitted electron energy distribution. Using this equation, we study the effect of the cathode surface potential barrier on the electron energy distribution and obtain the surface barrier parameters from the fit of the measured electron energy distribution curve (EDC) of the transmission-mode cathode. The theoretical result is in good agreement with the experimental result.

* Project supported by the National Natural Science Foundation of China (No. 60678043), the Natural Science Foundation of Jiangxi Province (No. 2007GQS0412), and the Research Foundation of Education Bureau of Jiangxi Province (No. GJJ08298)
† Corresponding author. Email: bkchang@mail.njust.edu.cn
Received 10 November 2007, revised manuscript received 20 April 2008

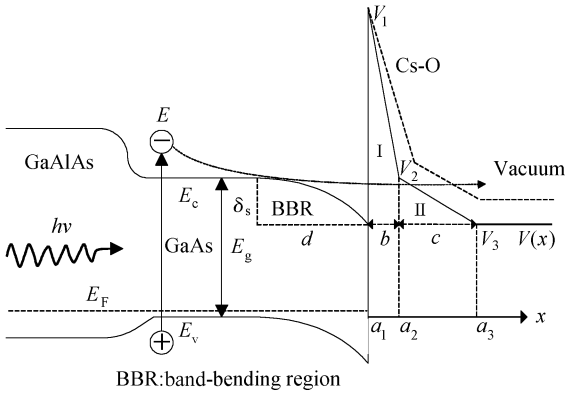

Fig. 1 Band structure and surface barrier for a typical transmission-mode NEA GaAs photocathode E_c is the conduction band minimum, E_v is the valence band peak level, E_g is the width of the band gap, E_F is the Fermi level, δ_s is the height of the surface band-bending, d is the width of the surface band-bending, V_1 is the start height of barrier Ⅰ, V_2 and V_3 are the end height of barriers Ⅰ and Ⅱ (V_3 is actually the vacuum level), and b and c are the thickness of barriers Ⅰ and Ⅱ.

2 Energy distribution of electrons reaching the cathode surface

The band structure and surface barrier for a typical transmission-mode GaAs photocathode are shown in Fig. 1. The profile of the surface barrier comprises two approximately straight lines with different slopes, which we call barriers Ⅰ and Ⅱ. This profile is proposed based on the double-dipole (dipoles Ⅰ and Ⅱ) model[11]. Barriers Ⅰ and Ⅱ are created by the dipoles Ⅰ and Ⅱ, respectively. The transmission coefficient of photoelectrons tunneling through the surface barrier is a function of the incident electron energy and surface barrier profile. Accordingly, before calculating the emitted electron energy distribution, the energy distribution of electrons reaching the cathode surface must be obtained.

The energy distribution of electrons in the conduction band at the onset of the surface band-bending region is determined by a Boltzmann distribution[9,12]. However, due to the energy lost by the electrons in traversing the band-bending region, the energy distribution of electrons reaching the surface changes. According to the work by Escher *et al.*[9,13,14], we calculate the energy distribution of electrons reaching the cathode surface at room temperature, as shown in Fig. 2. In the calculations, the following parameters are used[9,15]: the band gap $E_g = 1.42$eV, the energy loss per collision $\Delta E_p = 35$meV, the amount of band bending $\delta_s \approx E_g/3$, the relative dielectric constant for GaAs is taken to be $\varepsilon = 13.2$, and the doping concentration $n_A = 1\times10^{19}\,\mathrm{cm}^{-3}$.

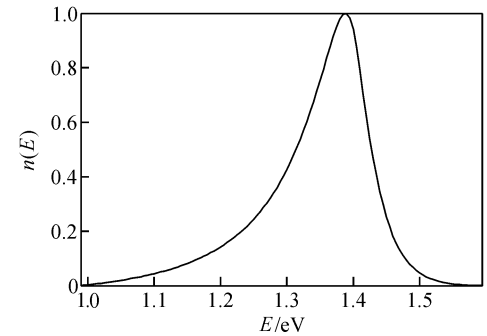

Fig. 2 Energy distribution of electrons reaching the cathode surface E is the incident electron energy and $n(E)$ is the electron energy distribution.

3 Probability of electrons tunneling through surface barrier

Since there is a Cs-O barrier on the cathode surface, only a part of the electrons reaching the surface can be emitted into the vacuum[12]. The probability that electrons emit into the vacuum is related to an energy-dependent transmission coefficient determined by the shape of the surface barrier. The transmission coefficient can be solved from the one-dimensional Schrödinger equation. However, only for some simple barrier structures, such as a rectangle barrier, the coefficient can be exactly solved. When an exact solution of the Schrödinger equation across a particular barrier is not available, a conventional method of solution is via approximation or numerical methods, such as WKB or finite-difference methods. These methods are approximate and inefficient[16]. In this work, a powerful method for solving the Schrödinger equation using piece-linear potential has been adopted, which is based on the Airy function. With this method, the coefficient can be accurately solved[16].

Figure 1 shows that the surface barrier comprises two piece-linear potential barriers, then the surface potential function is

$$V(x) = -F_i(x - b_i) \tag{1}$$

where $i = 1, 2$, $a_i < x < a_{i+1}$, $b_i = a_i + V_i/F_i$, $F_i = -(V_{i+1} - V_i)/(a_{i+1} - a_i)$.

The one-dimensional time-independent Schrödinger wave equation in barriers Ⅰ and Ⅱ is given by

$$\frac{\mathrm{d}^2\Psi(x)}{\mathrm{d}^2x} - \frac{2m}{\hbar^2}[V(x) - E]\Psi(x) = 0 \tag{2}$$

Because $V(x)$ is a piecewise-linear potential function, the solution of the Schrödinger equation across the intervals (a_1, a_2) and (a_2, a_3) can be expressed as a linear combination of the Airy function, then $\Psi_i(x)$ will be given as

$$\Psi_i(x) = C_i^+ Ai(z_i) + C_i^- Bi(z_i) \tag{3}$$

with $i = 1, 2$, $z_i = r_i(x - c_i)$, $r_i = -(2mF_i/\hbar^2)^{1/3}$, c_i

$= a_i + (V_i - E)/F_i$. Here Ai and Bi are the Airy function, C_i^+ and C_i^- are the coefficients to be determined, m is the electron effective mass, E is the incident electron energy, and $\hbar$ is the reduced Plank's constant.

In the regions $x < a_1$ and $x > a_3$, as shown in Fig. 1, the wave function is the free particle solution of the Schrödinger equation as follows:

$$\Psi_0(x) = C_0^+ \exp[ik_0(x - a_1)] + C_0^- \exp[-ik_0(x - a_1)], \quad x < a_1 \tag{4}$$

$$\Psi_3(x) = C_3^+ \exp[ik_3(x - a_3)] + C_3^- \exp[-ik_3(x - a_3)], \quad x > a_3 \tag{5}$$

where $k_0 = \sqrt{2mE}/\hbar$, $k_3 = \sqrt{2m(E - V_3)}/\hbar$, and C_0^+, C_0^-, C_3^+ and C_3^- are the coefficients to be determined.

At the interface a_{i+1}, particle conservation requires the continuity of the wave function, while momentum conservation demands the continuity of the derivative of the wave function, so the boundary conditions are given by

$$\Psi_i(x)\big|_{x=a_{i+1}} = \Psi_{i+1}(x)\big|_{x=a_{i+1}} \tag{6}$$

$$\left.\frac{d\Psi_i(x)}{dx}\right|_{x=a_{i+1}} = \left.\frac{d\Psi_{i+1}(x)}{dx}\right|_{x=a_{i+1}} \tag{7}$$

Upon applying boundary conditions to Eqs. (3)~(5), we can combine our results into one single transfer matrix equation that connects the coefficients of the wave functions C_0^+ and C_0^- in GaAs bulk with the coefficients of the wave functions C_3^+ and C_3^- in the vacuum to yield:

$$\begin{bmatrix} C_0^+ \\ C_0^- \end{bmatrix} = \begin{bmatrix} M_{11} & M_{12} \\ M_{21} & M_{22} \end{bmatrix} \begin{bmatrix} C_3^+ \\ C_3^- \end{bmatrix} = \frac{1}{2} \begin{bmatrix} 1 & -\frac{i}{k_0} \\ 1 & \frac{i}{k_0} \end{bmatrix} \times \begin{bmatrix} Ai(r_1(a_1 - c_1)) & Bi(r_1(a_1 - c_1)) \\ r_1 Ai'(r_1(a_1 - c_1)) & r_1 Bi'(r_1(a_1 - c_1)) \end{bmatrix} \times \begin{bmatrix} Ai(r_1(a_2 - c_1)) & Bi(r_1(a_2 - c_1)) \\ r_1 Ai'(r_1(a_2 - c_1)) & r_1 Bi'(r_1(a_2 - c_1)) \end{bmatrix}^{-1} \times \begin{bmatrix} Ai(r_2(a_2 - c_2)) & Bi(r_2(a_2 - c_2)) \\ r_2 Ai'(r_2(a_2 - c_2)) & r_2 Bi'(r_2(a_2 - c_2)) \end{bmatrix} \times \begin{bmatrix} Ai(r_2(a_3 - c_2)) & Bi(r_2(a_3 - c_2)) \\ r_2 Ai'(r_2(a_3 - c_2)) & r_2 Bi'(r_2(a_3 - c_2)) \end{bmatrix}^{-1} \times \begin{bmatrix} 1 & 1 \\ ik_3 & -ik_3 \end{bmatrix} \begin{bmatrix} C_3^+ \\ C_3^- \end{bmatrix} \tag{8}$$

where $F_1 = -(V_2 - V_1)/b$, $r_1 = -(2mF_1/\hbar^2)^{1/3}$, $c_1 = a_1 + (V_1 - E)/F_1$, $F_2 = -(V_3 - V_2)/c$, $r_2 = -(2mF_2/\hbar^2)^{1/3}$, $c_2 = a_2 + (V_2 - E)/F_2$.

Since there is no reflection in the vacuum, the coefficient C_3^- is zero and Equation (8) is rewritten as

$$\begin{bmatrix} C_0^+ \\ C_0^- \end{bmatrix} = \begin{bmatrix} M_{11} & M_{12} \\ M_{21} & M_{22} \end{bmatrix} \begin{bmatrix} C_3^+ \\ 0 \end{bmatrix} \tag{9}$$

Then the transmission coefficient $T(E)$ is given by

$$T(E) = \frac{k_3}{k_0} \left| \frac{1}{M_{11}} \right|^2 \tag{10}$$

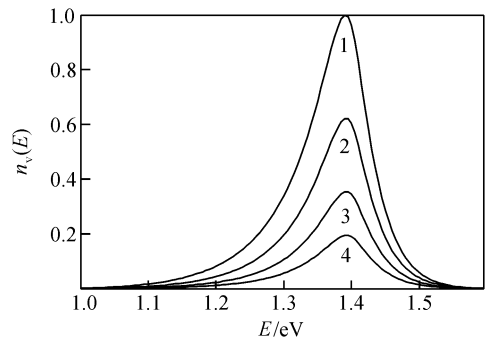

Fig. 3 Electron energy distribution of the cathode as a function of b b used in curves 1, 2, 3, and 4 are 0.05, 0.10, 0.15, and 0.20nm, respectively. Let $c = 0.7$nm, $V_2 = 1.42$eV, $V_3 = 0.9$eV.

The transmission coefficient $T(E)$ can now be computed as a function of the incident electron energy, the barrier height and thickness. For NEA cathodes, $T(E)$ is the probability of photoelectrons with energy E tunneling through surface barrier, generally denoted by

$$P(E) = \frac{k_3}{k_0} \left| \frac{1}{M_{11}} \right|^2 \tag{11}$$

4 Effect of surface barrier on emitted electron energy distribution

Because the energy distribution $n(E)$ of electrons reaching the cathode surface and the probability $P(E)$ of electrons tunneling through the surface barrier are known, the emitted electron energy distribution $n_v(E)$ can be obtained.

$$n_v(E) = n(E)P(E) \tag{12}$$

According to Eq. (12), we can simulate the effect of surface barrier on the emitted electron energy distribution. In the simulations, $n_v(E)$ is calculated in 10meV steps from $E = 1$ to 1.6eV. Figure 2 shows that when the electron energy is under 1eV or above 1.6eV, contributions to the energy distribution become negligible. The start height of barrier Ⅰ V_1 is taken as 4.9eV[17], which is generally a constant.

Figures 3 and 4 show a series of theoretical EDC as a function of different barrier-Ⅰ thicknesses and end heights, respectively. With the increase in barrier-Ⅰ thickness or end height, the surface-electron escape probability decreases quickly, and, accordingly, the number of emitted electrons reduces quickly also. The effect of the thickness on the emission of electrons is more pronounced. However, there is almost no effect of the increase in barrier-Ⅰ thickness or end height on the energy spread of the emitted electrons.

Figures 5 and 6 show a series of theoretical EDC as a function of different barrier-Ⅱ thicknesses and end heights, respectively. With the increase in barrier-

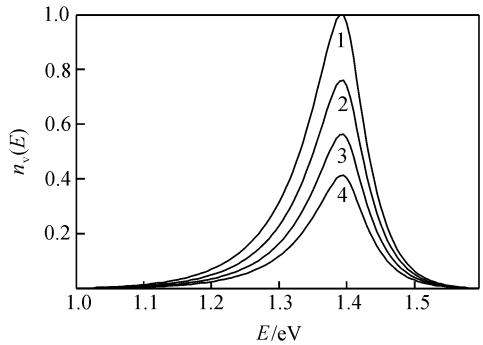

Fig. 4 Electron energy distribution of the cathode as a function of V_2 V_2 used in curves 1, 2, 3, and 4 are 1.3, 1.4, 1.5, and 1.6eV, respectively. Let $b = 0.15$nm, $c = 0.7$nm, $V_3 = 0.9$eV.

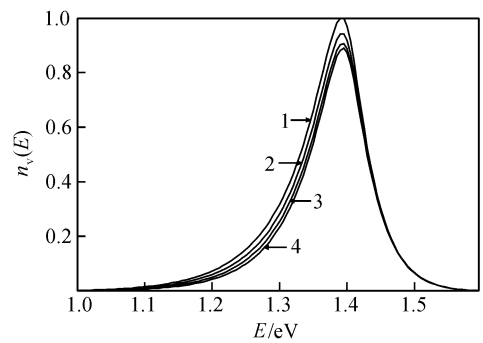

Fig. 5 Electron energy distribution of the cathode as a function of c c used in curves 1, 2, 3, and 4 are 0.6, 0.7, 0.8, and 0.9nm, respectively. Let $b = 0.15$nm, $V_2 = 1.42$eV, $V_3 = 0.9$eV.

Ⅱ thickness or end height, the number of emitted electrons with low energy decreases, while there is only a slight effect of the increase on the emission of the high energy electrons. The cut-off energy of the emitted electrons increases with the increase in the barrier-Ⅱ end height (vacuum level), and, accordingly, the energy spread of the emitted electrons narrows. However, the narrower energy spread sacrifices a certain amount of cathode quantum efficiency.

From these simulations of EDC as a function of surface barrier, we find changes in barrier Ⅰ mainly influence the quantum efficiency of cathodes, while

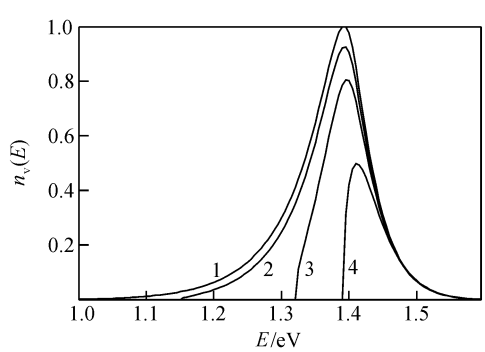

Fig. 6 Electron energy distribution of the cathode as a function of V_3 V_3 used in curve 1, 2, 3, and 4 are 0.9, 1.15, 1.32, and 1.39eV, respectively. Let $b = 0.15$nm, $c = 0.7$nm, $V_2 = 1.42$eV.

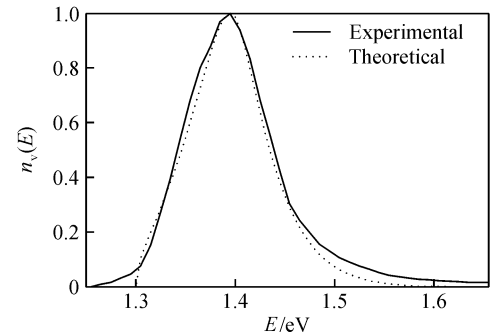

Fig. 7 Experimental and theoretical electron energy distribution of transmission-mode GaAs cathode Experimental conditions: $\lambda = 633$nm, $T = 300$K, $n_A = 1 \times 10^{19}$ cm^{-3}. Let $V_1 = 4.9$eV.

changes in barrier Ⅱ influence both the quantum efficiency and the energy spread. There is a contradiction in improving the quantum efficiency and narrowing the energy spread. To narrow the energy spread, the vacuum level should increase. However, in order to improve the quantum efficiency, the vacuum level should decrease. If the narrow energy spread is more important for an electron source, the optimal vacuum level should be a little lower than the conduction band minimum and the incident photon energy should be a little above E_g.

5 Surface barrier parameters fitted from electron EDC

The electron EDC can be calculated as a function of surface barrier parameters, and the barrier parameters can also be fitted from the measured EDC. The experimental EDC of the transmission-mode GaAs cathode are shown in Fig. 7, as measured by Baum *et al*.[8]. According to the experimental EDC, we obtain 41 raw energy distribution data points in 10meV steps, and using Eq. (12), the corresponding theoretical data points are calculated as a function of V_2, V_3, b, and c. According to the non-linear least square method, the theoretical (best-fit) EDC can be obtained from the fit of experimental EDC as the dashed line in Fig. 7. The theoretical curve is in good agreement with the experimental curve. The deviation in high energy electrons are related to the high energy (1.96eV) incident photons. The fitted thicknesses of barriers Ⅰ and Ⅱ are 0.114 and 0.6nm, respectively. The fitted end height of barriers Ⅰ and Ⅱ are 1.43 and 1.30eV, respectively. These fitted surface barrier parameters are significant in the characterization of the Cs-O activation layer of the cathode.

6 Conclusion

Based on the equation used to calculate the emit-

ted electron energy distribution of transmission-mode NEA GaAs photocathodes, the effect of the cathode surface potential barrier on the electron energy distribution is investigated. The barrier-Ⅰ thickness or end height has a significant effect on the quantum efficiency of the cathode, while barrier Ⅱ has a more pronounced effect on the electron energy spread. An increase in the vacuum level will lead to a narrower electron energy spread, while sacrificing a certain amount of cathode quantum efficiency. Using the equation, we also fit the measured EDC of the transmission-mode cathode and obtain the surface barrier parameters. The results and analysis methods of this study provide a reference for the performance improvement of electron sources and provide a new tool to investigate the surface properties of NEA cathodes.

References

[1] Wang Xiaofeng, Zeng Yiping, Wang Baoqiang, et al. High-integrated-photosensitivity negative-electron-affinity GaAs photocathodes with multilayer Be-doping structure. Chinese Journal of Semiconductors, 2005, 26(9): 1692

[2] Yan Jinliang, Xiang Shiming. Studies of glass-bonded GaAs transmission photocathode by double crystal X-ray diffraction. Chinese Journal of Semiconductors, 1998, 19(9): 678

[3] Zou Jijun, Chang Benkang, Yang Zhi, et al. Stability of GaAs photocathodes under different intensities of illumination. Acta Physica Sinica, 2007, 56(10): 6109

[4] Estrera J P, Bender E J, Giordana A, et al. Long lifetime generation IV image intensifiers with unfilmed microchannel plate. Proc SPIE, 2000, 4128: 46

[5] Schneider J E, Sen P, Pickard D S, et al. Patterned negative electron affinity photocathodes for maskless electron beam lithography. J Vac Sci Technol B, 1998, 16(6): 3192

[6] Alley R, Aoyagi H, Clendenin J, et al. The Stanford linear accelerator polarized electron source. Nucl Instrum Meth Phys Res A, 1995, 365: 1

[7] Yamamoto N, Yamamoto M, Kuwahara M, et al. Thermal emittance measurements for electron beams produced from bulk and superlattice negative electron affinity photocathodes. J Appl Phys, 2007, 102(2): 024904

[8] Baum A W, Spicer W E, Pease R F W, et al. Negative electron affinity photocathodes as high-performance electron sources Part 2: energy spectrum measurements. Proc SPIE, 1995, 2550: 189

[9] Escher J S, Schade H. Calculated energy distributions of electrons emitted from negative electron affinity GaAs: Cs-O surfaces. J Appl Phys, 1973, 44(12): 5309

[10] Drouhin H J, Hermann C, Lampel G. Photoemission from activated gallium arsenide I: very-high-resolution energy. Phys Rev B, 1985, 31(6): 3859

[11] Su C Y, Spicer W E, Lindau I. Photoelectron spectroscopic determination of the structure of (Cs, O) activated GaAs(110) surfaces. J Appl Phys, 1983, 54(3): 1413

[12] Fisher D G, Enstrom R E, Escher J S, et al. Photoelectron surface escape probability of (Ga, In) As: Cs-O in the 0.9 to ~1.6μm range. J Appl Phys, 1972, 43(9): 3815

[13] Bartelink D J, Moll J L, Meyer N L. Hot-electron emission from shallow p-n junction in silicon. Phys Rev, 1963, 130(3): 972

[14] Williams B F, Simon R E. Direct measurement of hot electron-phonon interactions in GaP. Phys Rev Lett, 1967, 18(13): 485

[15] Herrera-Gómez A, Spicer W E. Physics of high intensity nanosecond electron source. Proc SPIE, 1993, 2022: 51

[16] Wayne W L, Masao F. Exact solution of the Schrodinger equation across an arbitrary one-dimension piecewise-linear potential barrier. J Appl Phys, 1986, 60(5): 1555

[17] Spicer W E, Herrera-Gómez A. Modern theory and application of photocathodes. Proc SPIE, 1993, 2022: 18

表面势垒形状对 NEA 光阴极电子能量分布的影响*

邹继军[1,2] 杨 智[2] 乔建良[2] 常本康[2,†] 曾一平[3]

(1 东华理工大学电子工程系, 抚州 344000)
(2 南京理工大学电子工程与光电技术学院, 南京 210094)
(3 中国科学院半导体研究所, 北京 100083)

摘要: 通过计算电子到达阴极面时的能量分布和求解电子隧穿表面势垒的薛定谔方程得到了透射式 NEA GaAs 光阴极发射电子能量分布的计算公式. 利用该公式仿真研究了阴极表面势垒形状对电子能量分布的影响, 发现Ⅰ势垒变化对阴极的量子效率影响显著, 其中尤以Ⅰ势垒宽度影响更大, 而Ⅱ势垒则影响阴极的能量展宽, 其中真空能级的升高可使阴极电子能量分布更集中, 但却牺牲了一定的阴极量子效率. 拟合分析了实验测试的透射式阴极电子能量分布曲线, 实验与理论曲线吻合得很好, 并得到了阴极的表面势垒参数.

关键词: NEA 光阴极; 表面势垒; 透射系数; 电子能量分布; 量子效率
PACC: 7960; 7335C; 7280E
中图分类号: TN223 **文献标识码:** A **文章编号:** 0253-4177(2008)08-1479-05

* 国家自然科学基金(批准号:60678043), 江西省自然科学基金(批准号:2007GQS0412)和江西省教育厅科技计划(批准号:GJJ08298)资助项目

† 通信作者. Email: bkchang@mail.njust.edu.cn

2007-11-10 收到, 2008-04-20 定稿